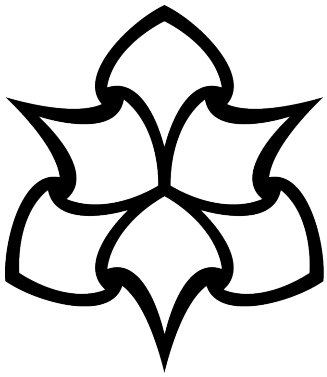

Electronics and Electrical Engineering

AIMS Electronics and Electrical Engineering, 2(3): 103–116.
DOI: 10.3934/ElectrEng.2018.3.103
Received: 11 July 2018
Accepted: 04 October 2018
Published: October 2018

http://www.aimspress.com/journal/ElectronEng

Research article

Optical environmental sensing in wireless smart meter network

Minglong Zhang[1], Iek Cheong Lam[2], Arun Kumar[3], Kin Kee Chow[2,*] and Peter Han Joo Chong[3]

[1] Department of Electrical and Electronic Engineering, Auckland University of Technology, New Zealand

[2] School of Engineering, Manchester Metropolitan University, United Kingdom

[3] School of Electrical and Computer Engineering, National University of Singapore, Singapore

* **Correspondence:** Email: K.Chow@mmu.ac.uk; Tel: +44(0)1612471632.

Abstract: In recent years, the traditional power grid is undergoing a profound revolution due to the advent and development of smart grid. Many hard and challenging issues of the traditional grid such as high maintenance costs, poor scalability, low efficiency, and stability can be effectively handled and solve in the wireless smart grid (WSG) by utilizing the modern wireless sensor technology. In a WSG, data are collected by sensors at first and then transmitted to the base station through the wireless network. The control centre is responsible for taking actions based on this received data. Traditional sensors are failing to provide accurate and reliable data in WSG, and optical fiber based sensor are emerging as an obvious choice due to the advancement of optical fiber sensing technology, accuracy, and reliability. This paper presents a WSG platform integrated with optic fiber-based sensors for real-time monitoring. To demonstrate the validity of the concept, fresh water sensing of refractive index (RI) was first experimented with an optical fiber sensor. The sensing mechanism functions with the reflectance at the fiber's interface where reflected spectra's intensity is registered corresponding to the change of RI in the ambient environment. The achieved sensitivity of the fabricated fiber sensor is 29.3 dB/RIU within the 1.33–1.46 RI range. An interface between the measured optical spectra and the WSG is proposed and demonstrated, and the data acquired is transmitted through a network of wireless smart meters.

Keywords: smart grid; wireless sensor networks; optical fiber sensors; environmental monitoring

1. Introduction

In traditional electric power grid system, large central generating stations are connected through a high-voltage (HV) transmission system. The transmission system is then connected to a distribution system that directly meets customer demand. In recent years, the transmission system has grown from local and regional grids into a large interconnected network. In traditional power grid, peak demand and energy consumption grew at predictable rates, and technology evolved in a relatively well-defined operational and regulatory environment. With current power grid systems gradually progressing into more advanced complexes, there are also many all around the world as we speak which are rendered archaic alternatively. In addition, the lack of modern technology has clearly outlined the limitations of large conventional power grids, drawing out problems it suffers such as energy loss, overload conditions, power quality issues, poor peak load management and time wastage on manual operation. In order to solve these problems, many research works have been carried out to upgrade the electric grid to a smart grid. The goal of the smart grid is to provide a much more reliable distribution, improve fault detection with self-healing capabilities of the network without the intervention of technicians, create greater efficiencies in monitoring and load adjustments based on peak using times and locations, provide better security to the grid, and empower the consumer to be able to better manage their usage and costs [1].

Wireless communication and networking are widely adopted in many smart grids due to its high flexibility and low complexity while keeping the costs low. Figure 1 illustrates an overview of a typical wireless smart grid architecture. In a wireless smart grid, data is first collected by different types of sensors and then sent to the base station through wireless networks. A smart grid sensor, which serves as a detection node, can enable the remote monitoring of equipment such as transformers and power lines. For instance, smart grid sensors can monitor weather and power line conditions which determine the line's carrying capacity, also known as dynamic line rating. This process can enable power companies to understand their power line's capabilities and ultimately helps them improve their efficiency as well.

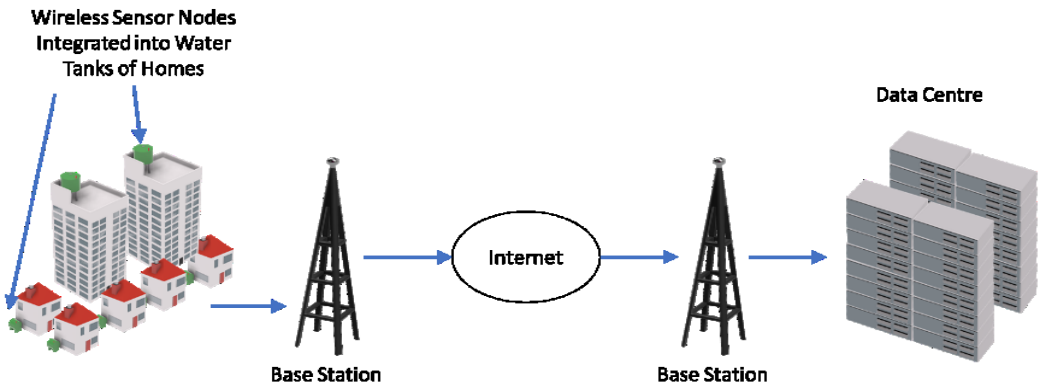

Figure 1. An overview of wireless smart grid architecture.

2. Comparison of sensors

Sensors based on Micro-Electro-Mechanical System (MEMS) have been traditionally used to acquire information on parameters such as temperature, pressure, acceleration, vibration and the measurement of chemical species [2]. Though, these MEMS sensors are tiny in size with low power consumption they have limitations in their measurement capabilities due to the limited types of sensing mechanisms built into these MEMS sensor designs [3,4]. Also, most of MEMS-based sensors have limited sensitivities thus making them less suitable for applications where high-sensitivity is required in the measurement.

As compared to MEMS-based sensors, optical fiber sensors are also small in size and lightweight, immune to electromagnetic interference, resistant to harsh condition and capable of distributed/quasi-distributed sensing with remote sensing capability which makes them suitable for high sensitivity applications [5]. Recently, optical fiber-based sensors are emerging as an obvious choice due to the advancement of optical fiber sensing technology, accuracy, and reliability and in most of the applications, optical fiber sensors have demonstrated significant advantages over conventional sensor technology, i.e., MEMS [6]. Uses of optical fiber sensors are limited in a wireless network and thus the benefits of the advanced design and the significant capabilities of optical fiber sensors are not fully utilised. Also, there has been limited research work on integration of optical sensors into a wireless network except some work on its integration into a wireless sensor network (WSN) platform [7], for embedded instrumentation systems [8] for remote flood monitoring [9] using polymer optical fibers as liquid level sensors and for a variety of temperature, pressure and chemical measurements [10] using optical fiber-based Fabry-Perot filters.

As a counter to the problems suffered by large conventional power grids, this paper proposes a wireless smart grid platform integrated with optical fiber based sensors for real-time remote environmental monitoring. Optical fiber based refractive index (RI) sensor for fresh water was primarily investigated to validate the feasibility of the concept.

3. Fabrication of sensing probe

In our experiment, a carbon nanotube (CNT) deposited optical fiber sensor for RI sensing is adopted due to its capability of continuous sensing with enhanced sensitivity [11–13], which is essential for our application in WSG. The design of the fiber sensor head consists of three parts: a standard single mode fiber (SMF), a multimode fiber (MMF) segment with core and cladding diameters of 105 μm and 125 μm respectively, and a thin film of CNTs deposited on the end face of the MMF segment as illustrated in Figure 2(a). The purpose of the deposition of the CNT thin film is due to its high RI optical property which will empower and amplify the range of RIs [11–13]. The first stage of fabricating the sensing probe involves creating the main body of the sensing probe, where one end of the MMF segment is fusion spliced to the SMF. In the second stage, the SMF-MMF joint fiber segment is formed by cleaving the other end of the MMF segment to a length of 21 mm away from the SMF-MMF splicing point. In the next stage of CNT preparation, CNT powder is dissolved into dimethylformamide (DMF) solution which is then sonicated in an ultrasonic bath for around 30 hours. This will produce CNT in the form of a solution with the nanoparticles evenly dispersed. Finally, using an optical deposition procedure, CNTs are deposited at the end face

of the cleaved MMF segment [14,15]. By using this deposition method, the carbon nanomaterials would adhere strongly onto the fiber surface through van der Waal's forces forming a good durability of coating for practical applications [16]. Figure 2(b) shows a microscopy image of the CNT coated fiber end face. As mentioned previously, CNTs possesses a high RI and it will have an effect on the reflected spectrum. Figure 3 shows the reflected optical spectrum of the sensing probe before (black line) and after (blue line) the optical deposition of CNT at the SMF-MMF fiber segment. An increased in the intensity of the reflected spectrum due to the CNT deposition is observed, hence the variation of ambient RI can be recorded.

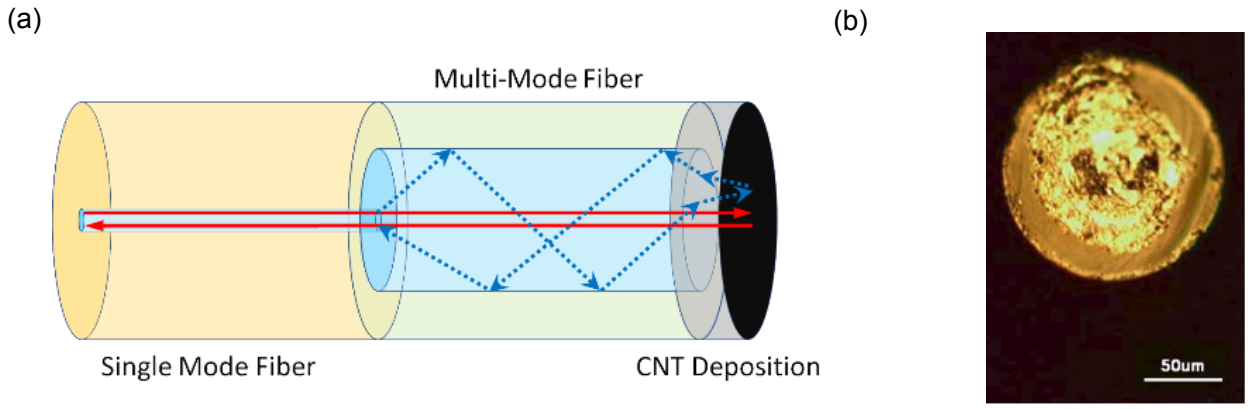

Figure 2. (a) Schematic illustration of the sensing probe fabricated with depositing carbon nanotubes (CNTs) onto a joint SMF-MMF fiber segment; and (b) microscopic image of CNT deposited on the end face of the joint fiber segment.

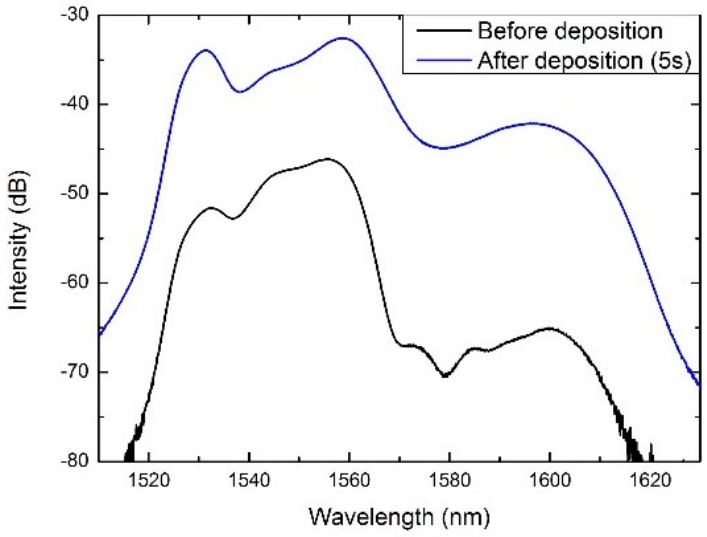

Figure 3. Measured reflected optical spectra of the joint fiber segment before and after CNTs deposition.

4. Measurement results of sensing probe

Before experimenting the performance of the fabricated sensing probe, certain requirements and control conditions should be met. For instance, to create the test solution with different RIs, a saturated sucrose solution is first produced through dissolving sugar into de-ionized water. Different sugar concentrations will possess different values of RI, hence it is the ideal test solutions for RI characterization utilizing the sensing probe as it will simulate the RI disturbances of a real external environment. The saturated sucrose solution is then divided to create a set of solutions with equal volume and concentration. Finally, through the addition of different volumes of DI water into each of the saturated sucrose solution, a set of sucrose solution with different sugar concentration is created as the test solutions. In our experiment, a constant environment at an ambient temperature of 23.7 ± 0.1 °C was occupied to ensure that the RI and temperature cross-coupling effects are kept at minimum. Before each RI characterization the sensing probe conducts on the test solutions, it was rinsed with DI water and dried. Furthermore, it was ensured that the air-exposed sensing probe's reflected spectrum was recovered before the next test. Figure 4 shows the experiment setup of the sensing probe measurement, which consists of the fabricated sensing probe, an optical circulator, a broadband source and an optical spectrum analyser (OSA). With a pipette, 1 ml of each test solution was placed on glass slides for the sensing probe to be submerged into. The SMF end of the sensing probe is connected to a broadband source through a circulator connected to an OSA to monitor the back reflected spectrum from the sensing probe. The intensity variation of the spectral features in the output spectra for each test solution was recorded on the OSA.

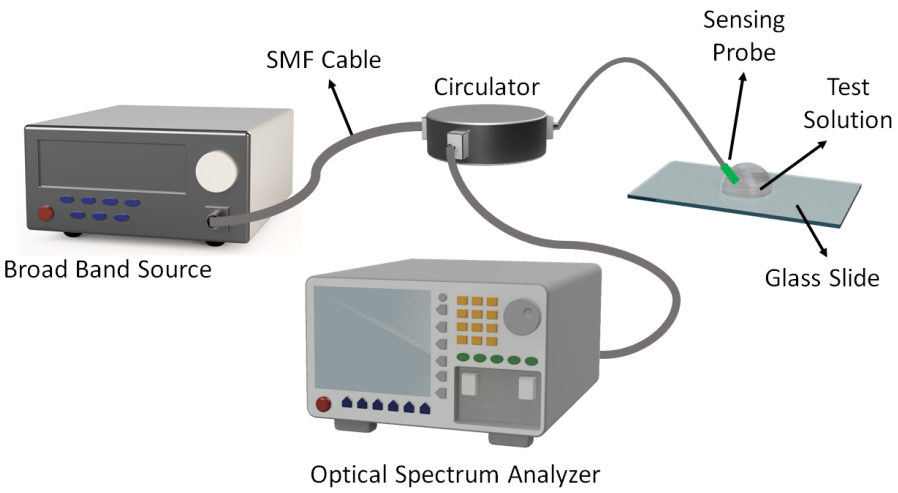

Figure 4. Experimental setup for the RI measurements with the fabricated sensing probe.

Figure 5 shows the recorded reflected spectra against RI variations of the test solutions from the sensor. An increase of the intensity of the reflected spectrum with the decrease of RI from the different concentrations of sucrose test solutions is observed.

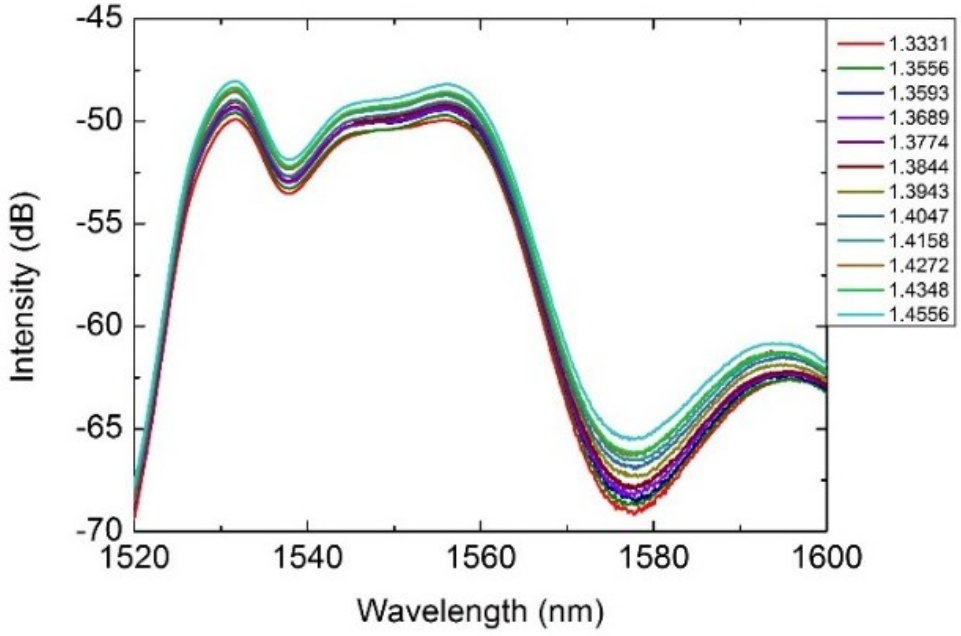

Figure 5. Reflected optical spectra of the fiber sensor corresponding to different RI of the ambient environment.

From the results shown in Figure 5, inside the ambient RI range 1.33 to 1.46, the intensity variation magnitude can be approximated to be ~3.8 dB with a sensitivity calculated to be 29.3 dB/RIU. With an intensity resolution of OSA of 0.01 dB, it is determined that the achievable resolution for the sensor is approximately ~3.4 × 10^{-4} RIU. It is believe that the sensitivity of the sensor can be further increase by shortening the length of MMF segment. However, it could be limited by the fusion splicer adopted in the experiment. After examining the performance of the sensing probe, the investigation proceeds to the practical application of WSG. As the WSG will only read electrical signals, an interface between the measurements of the optical spectra and the WSG is essential. In order to serve this purpose, the OSA is replaced by an optical tunable bandpass tuned centered at the interference dip at around 1580 nm of the output optical spectra, followed by an optical amplifier and photodetector. Through this setup, instead of recording the ambient RI variation through the shift in intensity of optical spectra, the ambient RI will be recorded as an output voltage change from the photodetector. Figure 6 shows a plot of the output voltage of the photodetector against the ambient RI of the fiber sensor. The data will then be sent into the wireless smart grid platform for transmission to the data center for further processing and analysis, and an interface between the optical sensing probe and the WSG is achieved. Besides the RI sensing as a proof of concept demonstration, practical applications into chemical sensing would also be explored. It has been shown that CNTs can be functionalized to allow certain molecules to bind to functionalized sites the CNTs [17,18]. By functionalizing the CNTs before deposition, various analyte specific optical fiber-based sensing probes can be fabricated, opening up the possibility for applications in chemical or bio-chemical sensing for environmental monitoring.

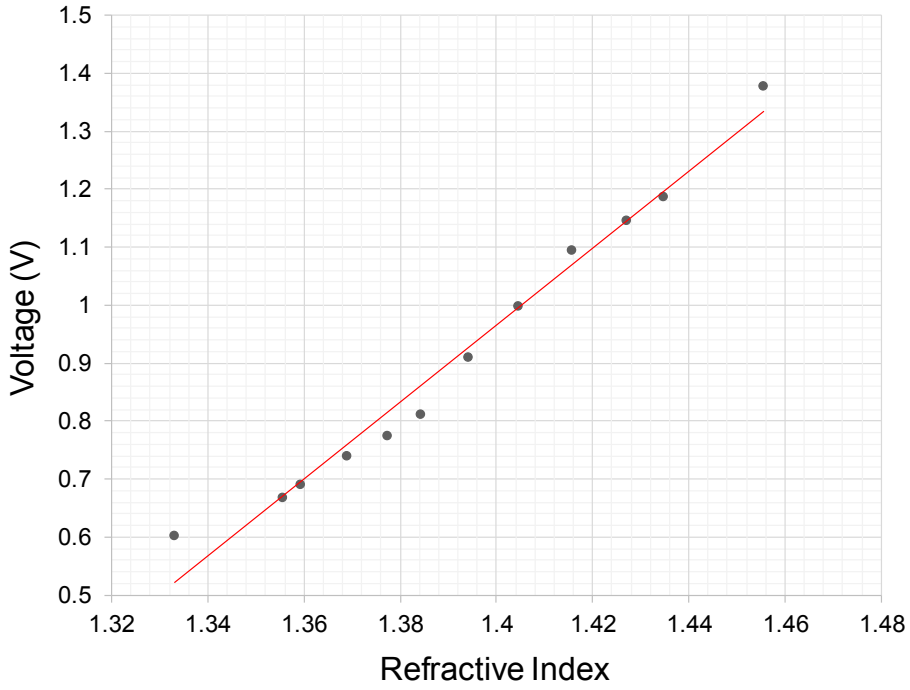

Figure 6. Plot of the output voltage of the photodetector corresponding to the various RIs of the external environment.

5. Wireless sensor network and performance analysis

In this section, WSN of the smart grid will be simulated to evaluate its performance. We first describe the system model and its performance metric and then demonstrate simulation results.

5.1. System model

A wireless sensor network usually consists of a number of sensors and a sink node. Each sensor node periodically generates a packet and transmits it to the sink. Due to the constraint of energy consumption in sensor nodes, their transmission range is limited to a relatively small range (e.g., 10 to 100 meters). Therefore, most of the sensor nodes cannot send data directly to the sink and intermediate nodes need to relay packets sent by their peers in order to deliver packets to the destination. Packets from remote nodes may even be relayed several times. During packet propagation, transmission collision is inevitable and it will result in packet loss. In order to tackle this issue, we add smart meters in the network. Each smart meter has a broader transmission range and their functionality is to forward data received from sensors to the sink. In our network, all nodes located in a particular region. Assume there are Ns sensors and Nsm smart meter in the region, and the period of generating and transmitting a packet is t_p, within a time T, if the sink receives P packets, the packet delivery ratio (PDR) is defined as:

$$PDR = \frac{t_p P}{TN_s} \tag{1}$$

In the following discussions and simulations, PDR is used as a performance metric to evaluate network performance.

Table 1. Key parameters in simulation

Parameter	Value
Packet Generation Frequency	One packet per second
Packet Size	128 bytes
Number of Sensor Nodes	20~120
Number of Smart Meter	4~8
Transmission Range	Sensor: 20~120 m
	Smart Meter: 250~350 m
Data Rate	128 kbps
Routing Algorithm	AODV
Path Loss Exponent	3.75

5.2. Simulation setup

The simulation setup accords with the system model described above. Sensor nodes randomly distribute in a specific region (e.g., a rectangle, a square or a disc), while smart meters uniformly locate at geometric centre of subregions (such as one-quarter of a rectangle or a square) to assure the best coverage of sensor nodes. A log-distance path loss model is incorporated in all channels. All key parameters are listed in Table. I. We run simulations for different WSNs in NS-3 [19] and compare the PDR performance with a benchmark of the same network without smart meters.

5.3. Simulation results

Figure 7 demonstrates how transmission range affects PDR performance in a WSN. In this simulation, 36 sensor nodes randomly distribute in a 200-by-200 m square, while the sink locates at the origin point. By utilizing four smart meters, the PDR performance is improved obviously. In addition, the improvement is more dramatic especially in the case of short transmission range. For

instance, when the transmission range is 20 m, the PDR almost triples if smart meters are employed in the network. The reason is that, with a low transmission power, some isolated nodes (i.e., the distance among adjacent nodes is larger than the communication range) cannot find a route to the sink. Thus, information generated by those isolated nodes is hard to be delivered. By contrast, by adding smart meters, those nodes may easily find a route to one of smart meters even if no direct route to sink exists. It is also true for the case of a broader communication range of sensor nodes, but the improvement is not as significant as the case of smaller communication range, because larger communication range can results in better connectivity among sensor nodes. Moreover, an overlarge transmission range (say 120 m) reduce the PDR because interference may be strong when more than on node is transmitting.

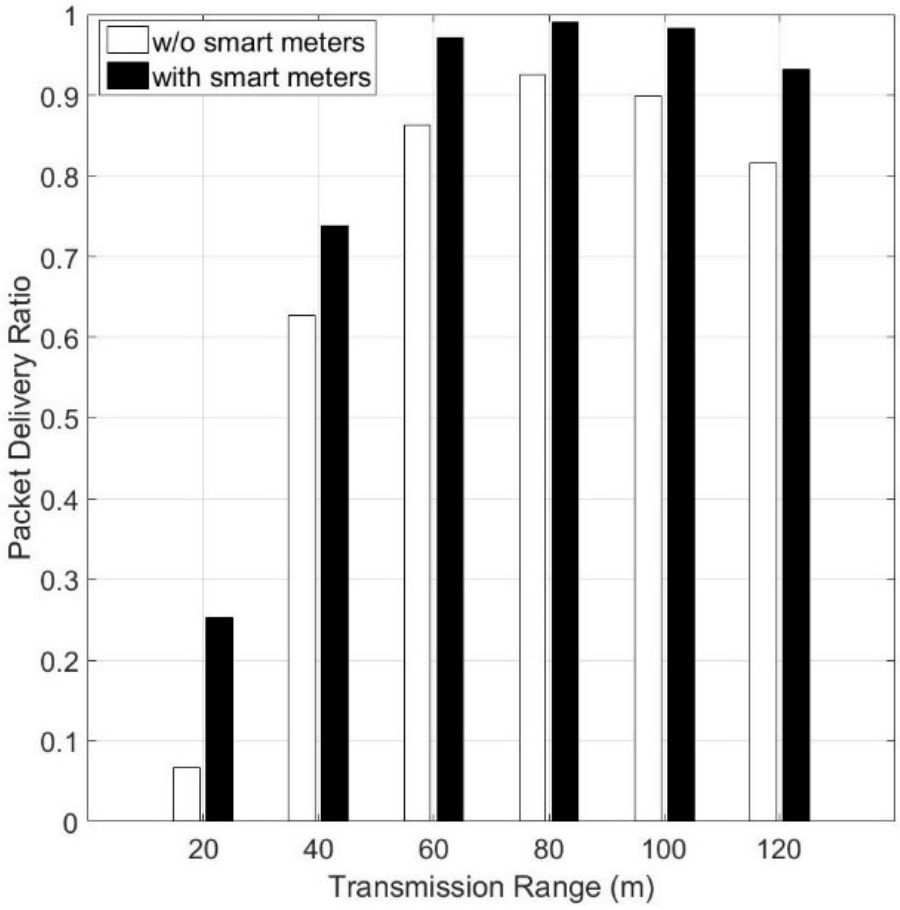

Figure 7. The PDR performance for different communication ranges of sensor nodes: the number of sensor nodes is 36 and the number of smart meters is 4. White bars are for a WSN without smart meters, while black ones for the network with smart meters.

Except for transmission range, the density of sensor nodes also influences the PDR performance, which is revealed in Figure 8. For this case, sensor nodes and four smart meters located at the same square but with the fixed transmission range of 40 m for all sensors. From the bar graph, we can see that the PDR performance firstly increases as the node density increases, but then it decreases when the density is too high (i.e., more than 100 nodes in the square), as high node density may cause

more transmission collisions. For a sparse network, it is hard for some isolated nodes to find a valid route to the sink or a smart meter. However, the occasion changes with more sensor nodes in the area because it makes higher probability of finding a route, since the average distance between neighboring nodes is reduced. In addition, adopting smart meter is effective to enhance PDR for the sparse WSN because those remote or isolated nodes have larger probability to communicate with the smart meter than with the sink.

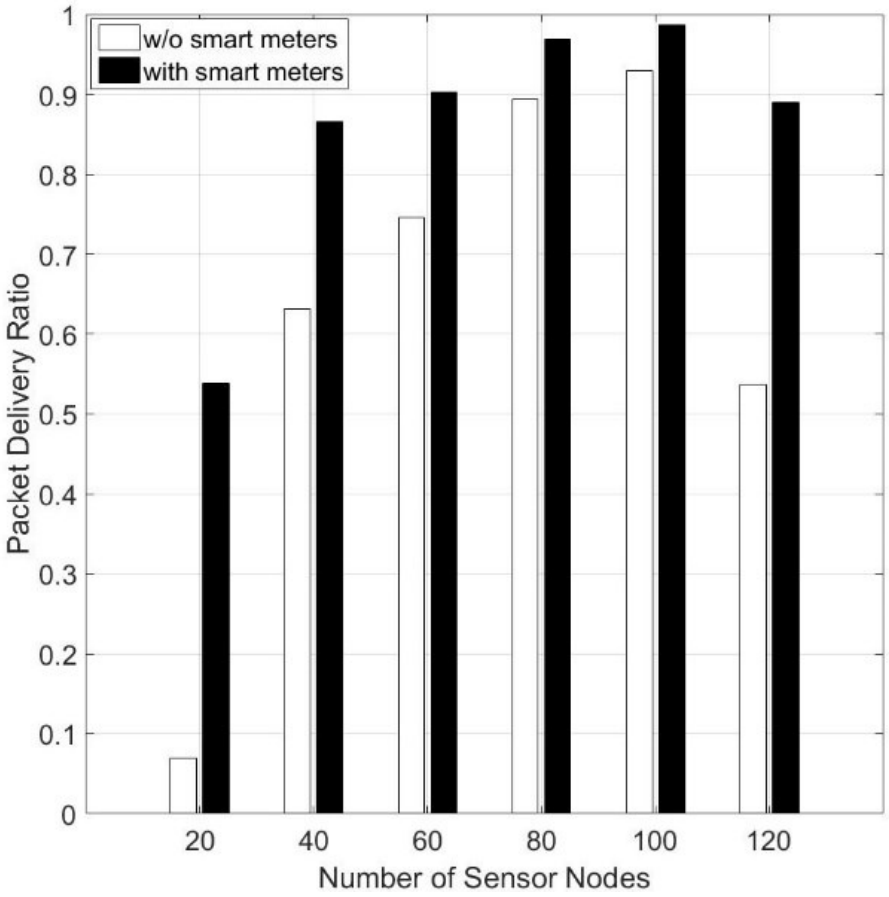

Figure 8. The PDR performance for different node density: the transmission range of each sensor node and smart meter is 40 m and 250 m, respectively.

To see how the number of smart meters affects the network performance, simulations are conducted in the same square and same configurations but with different amounts of smart meters. In Figure 9, the PDR rises steadily as the number of smart meters increases, which meets our expectation, because with more smart meters, data from sensor nodes can be more easily sent to the nearest smart meters, which is able to forward those information directly to the sink.

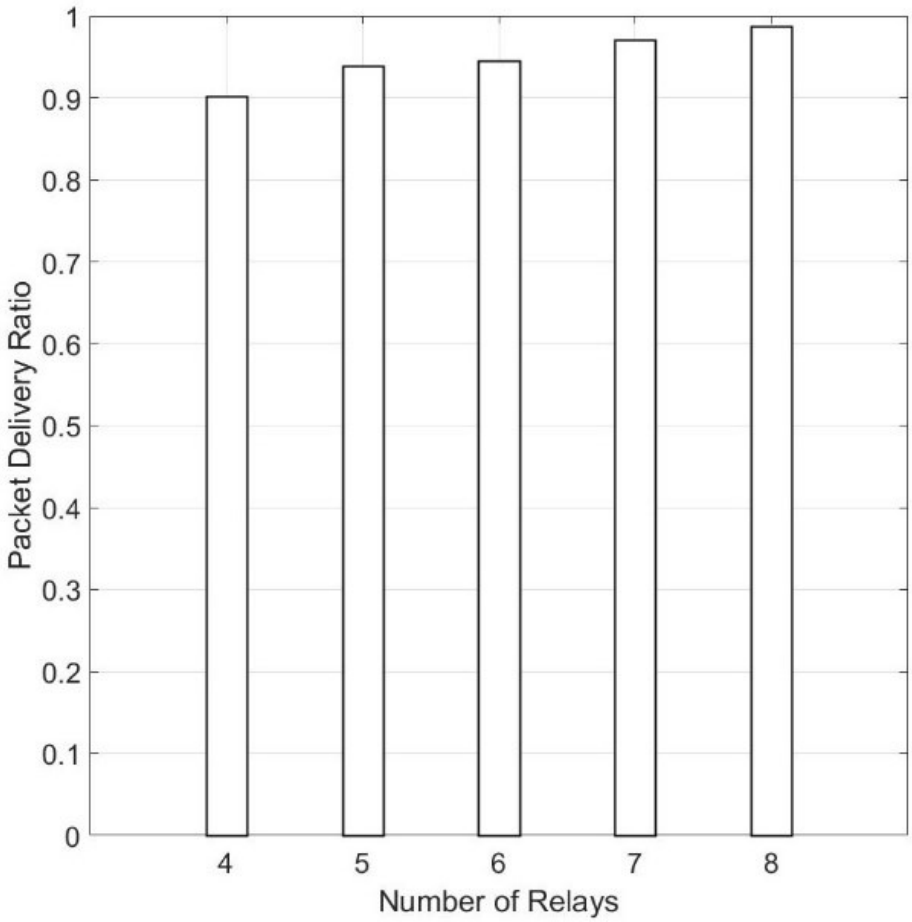

Figure 9. The PDR performance for networks with different numbers of smart meters: the transmission range of each sensor node and smart meter is 40 m and 250 m, respectively.

In the last, we compare the PDR performance for WSNs with different shapes (e.g., three rectangles, one square and one disc) of distribution regions but with the same node density. The number of sensor nodes and smart meters is 60 and 4, respectively. For sensor nodes, its transmission range is fixed to 40 m, but it varies for smart meters because different shapes have different requirements on the transmission ability of smart meters. From Figure 10, the PDR performance is boosted by smart meters for all shapes. In addition, it is apparent that for a rectangle, enlarging the proportion of its length and width will result in a lower PDR, which can be explained that disproportional rectangles increase the probability of generating isolated nodes under the condition of fixed transmission power. Similarly, smart meters are able to substantially improve the PDR, especially for extreme cases where the shape of the region is a disproportional rectangle.

Considering the feature of a wireless sensor network, the sensor nodes in all the above simulations randomly distribute in a particular area. Obviously, the sensor nodes hardly locate uniformly the reality. To enhance the PDR performance, two strategies are eligible: (1) deploying

more smart meters in the region, and (2) placing those meters uniformly in the region. Since the distribution of sensor nodes are in a random way, such placement of smart meters can increase the probability of route establishment for some remote or isolated nodes. The above conclusion are also proved by Figure 9 and Figure 10.

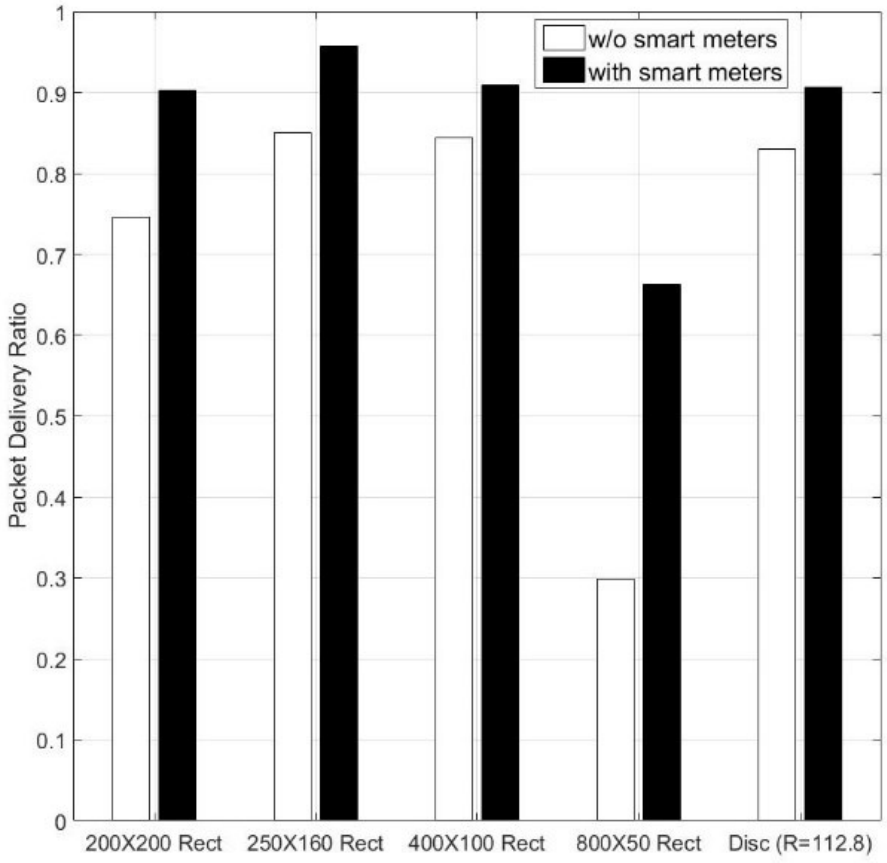

Figure 10. The PDR performance for WSNs (consisting of 60 sensor nodes and 4 smart meters) with different shapes**.**

6. Conclusion

In summary, integration of optical fiber based environmental sensor on wireless smart grid (WSG) platform has been proposed. As a proof-of-concept, an RI sensing probe, fabricated through fusion splicing a multimode fiber (MMF) segment to a single mode fiber (SMF) with carbon nanotubes (CNTs) onto the MMF end face, has been presented. The sensing probe displayed clear and distinct variations in its output spectra to perturbations in RI of its external environment. The achievable sensitivity is calculated to be 29.3 dB/RIU for the fabricated fiber sensor within the RI range of 1.33-1.46. An interface between the measured optical spectra and the WSG is proposed and demonstrated and the acquired data has been transmitted by the wireless smart meters. Thus, it can allow scalability of the sensing areas.

Conflict of interest

The authors declare no conflict of interests in this paper.

References

1. Mahmood A, Javaid N and Razzaq S (2015) A review of wireless communications for smart grid. *Renew Sust Energ Rev* 41: 248–260.
2. Yick J, Mukherjee B, Ghosal D (2008) Wireless sensor network survey. *Comput Netw* 52: 2292–2330.
3. Pakzad SN, Fenves GL, Kim S, et al. (2008) Design and Implementation of Scalable Wireless Sensor Network for Structural Monitoring. *J Infrastruct Syst* 14: 89–101.
4. Li X, Cheng X, Yan K, et al. (2010) A Monitoring System for Vegetable Greenhouses based on a Wireless Sensor Network. *Sensors* 10: 8963–8980.
5. Yeo TL, Sun T, Grattan KTV (2008) Fiber-optic sensor technologies for humidity and moisture measurement. *Sensor Actuat A-Phys* 144: 280–295.
6. Culshaw B (2004) Optical Fiber Sensor Technologies: Opportunities and Perhaps Pitfalls. *J Lightwave Technol* 22: 39–50.
7. O'Connell E, Healy M, OKeeffe S, et al. (2013) A Mote Interface for Fiber Optic Spectral Sensing With Real-Time Monitoring of the Marine Environment. *IEEE Sens J* 13: 2619–2625.
8. Lloyd SW, Newman JA, Wilding DR, et al. (2007) Compact optical fiber sensor smart node. *Rev Sci Instrum* 78: 35108.
9. Kuang KSC, Quek ST, Maalej M (2008) Remote flood monitoring system based on plastic optical fibers and wireless motes. *Sensor Actuat A-Phys* 147: 449–455.
10. Pang C, Yu M, Zhang XM, et al. (2012) Multifunctional optical MEMS sensor platform with heterogeneous fiber optic Fabry–Pérot sensors for wireless sensor networks. *Sensor Actuat A-Phys* 188: 471–480.
11. Tan YC, Ji WB, Mamidala V, et al. (2014) Carbon-nanotube-deposited long period fiber grating for continuous refractive index sensor applications. *Sensor Actuat B-Chem* 196: 260–264.
12 Tan YC, Tou ZQ, Mamidala V, et al. (2014) Continuous refractive index sensing based on carbon-nanotube-deposited photonic crystal fibers. *Sensor Actuat B-Chem* 202: 1097–1102.
13. Tan YC, Tou ZQ, Chow KK, et al. (2015) Graphene-deposited photonic crystal fibers for continuous refractive index sensing applications. *Opt Express* 23: 31286–31294.
14. Nicholson JW, Windeler RS, DiGiovanni DJ (2007) Optically driven deposition of single-walled carbon-nanotube saturable absorbers on optical fiber end-faces. *Opt Express* 15: 9176–9183.
15. Kashiwagi K, Yamashita S, Set SY (2009) In-situ monitoring of optical deposition of carbon nanotubes onto fiber end. *Opt Express* 17: 5711–5715.
16. Yamashita S (2012) A Tutorial on Nonlinear Photonic Applications of Carbon Nanotube and Graphene. *J Lightwave Technol* 30: 427–447.
17. Lee H, Shaker G, Naishadham K, et al. (2011) Carbon-nanotube loaded antenna-based ammonia gas sensor. *IEEE T Microw Theory* 59: 2665–2673.

18. Kruss S, Hilmer AJ, Zhang JQ, et al. (2013) Carbon nanotubes as optical biomedical sensors. *Adv Drug Deliver Rev* 65: 1933–1950.
19. The Network Simulator tool: ns-3. Available from: https://www.nsnam.org/.

AIMS Press